Chemical Engineering Journal 437 (2022) 135192

Contents lists available at ScienceDirect

Chemical Engineering Journal

journal homepage: www.elsevier.com/locate/cej

Performance of continuous-flow micro-reactors with curved geometries. Experimental and numerical analysis

Christian Fernández-Maza, Marcos Fallanza, Lucía Gómez-Coma, Inmaculada Ortiz *

Departamento de Ingenierías Química y Biomolecular, Universidad de Cantabria, Av. Los Castros s/n, 39005 Santander, Spain

ARTICLE INFO

Keywords:
Micro-reactor design
Mixing efficiency
Curved-shaped geometry
CFD modelling
Fluid phase reactions
Dean vortices

ABSTRACT

One of the major challenges in the design of micro-devices, when very fast reactions are carried out, is to overcome the limited performance due to the poor mixing efficiency of the reactants. Here, we report a holistic analysis of reactants mixing and reaction rate in liquid phase flow micro-reactors with curved geometries. In this sense, a mathematical model that accounts for momentum and mass conservation equations, together with species transport and chemical reaction rate under isothermal conditions, has been developed using computational fluid dynamics techniques (CFD). To validate the predictive model, four micro-reactor geometries with different radius and curved length (straight reactor, two types of serpentines and an Archimedean spiral) have been evaluated. Simulated results proved that mixing is promoted through the formation of Dean vortices as a consequence of the reduction of the radius of curvature and at the same time of the extension of the curve. Thus, the overall performance of the micro-reactor is improved because mass transport limitations are minimized and the process kinetics are greatly enhanced. Accordingly, the spiral micro-reactor reported the best performance by reducing by half the time required to obtain 95 % conversion when compared with the straight reactor. Simulated findings have been confirmed with the experimental analysis of the reaction between aqueous ammonium and hypochlorite ions. Very good agreement between simulated and experimental results has been achieved with an error lower than 10 %. Therefore, the robust model herein reported is a novel and valuable tool to assist in the optimum design of micro-reactors for fluid-phase isothermal applications.

1. Introduction

Microfluidics have attracted great attention among the scientific community due to their unique capabilities in the control of molecules concentrations in space and time offering new opportunities in multiple fields [1]. Different applications such as microextraction [2–5], magnetophoretic separations [6,7], gas–liquid absorption [8,9], detection of compounds of interest in food and biomedical applications [10–12], polymer synthesis [13], catalytic reactions [14–16], preparation of functionalized nanomaterials [17–19] and synthesis of active pharmaceutical ingredients [20–22] among others have been reported so far. The precise control of the reagents concentration, temperature and residence time results in more accurate estimation of the kinetic parameters [23–26] with micro-reactors. Moreover, these miniaturized chemical reactors have improved chemical synthesis towards the substitution of traditional batch reaction in flow chemistry systems [27–29]. However, for the implementation of chemical reactions, where reactants must get in contact, mixing represents often a challenge [30,31]. While active micro-mixers use external energy sources such as electric, acoustic or magnetic fields to promote mixing, the use of passive micro-mixers, whose performance relies solely on their geometry, has the advantages of lower operational cost and a less-complex fabrication process. In passive micro-mixers two physical principles can be used to induce mixing: diffusion and convection. When driven by diffusion, the only way to achieve mixing is by decreasing the diffusional path of the molecules. Nevertheless, when convection is the mechanism that controls mixing, it involves the detailed design of the micro-reactor's geometry to promote non-parallel flow field that finally leads to enhanced mixing of the molecules [32]. This facilitates overcoming diffusional limitations and results in increased throughput and product yield [33–35].

T-shape geometry has been deeply investigated in micro-mixers' literature since the beginning of 21st century. In 2000 Won et al.[36] fabricated micro-mixers in a silicon substrate and investigated the mixing performance. More recently, Camarri et al.[37], Nimafar et al. [38] and Viktorov et al.[39] investigated the mixing degree in three different geometries: T-micromixer, O-micromixer and H-micromixer.

* Corresponding author.
E-mail address: ortizi@unican.es (I. Ortiz).

https://doi.org/10.1016/j.cej.2022.135192
Received 26 November 2021; Received in revised form 18 January 2022; Accepted 7 February 2022
Available online 9 February 2022

Nomenclature

Roman Symbols

C_D	drag coefficient
C_i	molar concentration of specie i mol/m^3
D_i	molecular mass diffusivity m^2/s
$\vec{g}$	gravity acceleration m/s^2
$\vec{j_i}$	diffusion flux of species i $mol/(m^2 s)$
$M_{w,i}$	molecular weight of specie i kg/mol
p	pressure Pa
t	time s
$\vec{v}$	velocity m/s
Y_i	molar fraction of species i

Greek Symbols

μ	dynamic viscosity $kg/(ms)$
ρ	fluid density kg/m^3
ρ_i	mass concentration of species i kg/m^3
τ	stress tensor Pa
R_i	molar chemical generation of species i $mol/(m^3 s)$

Hsieh et al.[40] employed optical visualization techniques to investigate the mixing efficiency in Y-type micro-mixers as a function of the mixing angle. Yang et al.[41] and Hossain et al. [42] focused their work on the evaluation of the mixing performance of modified Tesla structures. They reported mixing efficiencies above 95% for Reynolds numbers below 100 and moderated pressure drops (less than 1054 Pa). The mixing performance of curved micro-channels has been widely studied in literature. In this case, inertial mixing can occur due to the formation of double Dean vortices which greatly improve the mixing efficiency. Alijani et al. [43] and Durydhan et al.[44] tested different curved geometries (serpentine and spiral shapes) and they concluded that the presence of Dean vortices enhanced the mixing performance with the mixing index reaching values around 95%. Many authors use these devices as micro-reactors in different applications such as the synthesis of ibuprofen studied by Bogdan et al.[20] in continuous-flow micro-reactors; the experimental procedure followed three steps and the authors reported 68% of yield. Also, Ghosh et al.[45] employed a micro-reactor to intensify and increase the efficiency of the enzymatic production of xilooligosaccharides and they achieved 12 times faster the same conversion of xylan to xylooligosaccharides compared to a conventional batch process by feeding the same reagent volume in both systems.

The literature contains interesting reports with the analysis of different geometries of passive micro-mixers different to the aforementioned geometries, either experimentally or described by CFD simulation techniques [46–48]. In general, the modification of micro-devices shape is the basic idea for splitting, stretching, folding and breaking of the flow, because increasing the contact surface area between the different fluid layers promotes the rate of mass transfer [48].

Thus, the interest and applications of flow micro-reactors demands a deep study that considers in an integrated way the analysis of mixing, component's mass transport and chemical reaction kinetics. This work aims to gain insight and model the coupling between mixing efficiency and chemical reaction kinetics in liquid-phase isothermal micro-reactors. A methodology for the analysis and design of micro-reactors has been developed based on CFD techniques and has been experimentally validated with the results of a very fast reaction implemented in four different micro-devices with curved geometries. The methodology herein reported as well as the conclusions obtained in this work can be extended to other geometries and operational conditions typically used in microfluidic systems for different applications.

2. Mathematical model

In order to quantify the solute's concentration at each point in the micro-device, and then evaluate the performance of the micro-reactors, the flow field, coupled to mass transport and chemical reaction equations must be solved.

The Navier-Stokes equations have been expressed in dimensionless form [49], with dimensionless variables as follows:

$$\phi' = \frac{\phi}{\phi_0}$$

where "ϕ" is the original variable with dimensions, "ϕ_0" is a dimensional constant (a characteristic value of the variable) and consequently, "ϕ'" is the dimensionless variable.

The dimensionless continuity equation can be written as follows:

$$S\frac{\partial \rho'}{\partial t'} + \nabla' \cdot (\rho' \vec{v}') = 0 \tag{1}$$

where "S" is the Strouhal number.

The dimensionless momentum equation is:

$$S\frac{\partial \rho' \vec{v}'}{\partial t'} + \nabla' \cdot (\rho' \vec{v}' \vec{v}') = -\mathrm{Eu}\nabla' p' + \frac{1}{\mathrm{Re}}\nabla' \cdot \tau' + \frac{1}{\mathrm{Fr}}\rho' \vec{g}' \tag{2}$$

where "Eu" is the Euler number, "Re" is the Reynolds number, "Fr" is the Froude number and "τ'" is the dimensionless stress tensor:

$$\tau' = \frac{1}{2}C_D \mathrm{Re} \tag{3}$$

where "C_D" is the drag coefficient:

$$C_D = \frac{\tau}{\frac{1}{2}\rho_0 \vec{v_0}^2} \tag{4}$$

and "τ" is the stress tensor (Pa) that is given by:

$$\tau = \mu\left[\left(\nabla \vec{v} + \nabla \vec{v}^T\right) - \frac{2}{3}\nabla \cdot \vec{v} I\right] \tag{5}$$

where "I" is the unit tensor and the second term on the right hand side is the effect of the volume dilation.

The generalized mass conservation equation for a chemical specie, when applied to a fluid–fluid mixture is:

$$S\frac{\partial \rho_i'}{\partial t'} + \nabla' \cdot (\rho_i' \vec{v}') = -\frac{1}{\mathrm{Pe}}\nabla' \cdot \vec{j_i}' + \mathrm{Da}R_i' \tag{6}$$

where "Pe" is the Péclet number, Da is the Damköhler number, "R_i'" is the dimensionless net rate of formation of component "i" due to chemical reaction and "$\vec{j_i}'$" is defined by Eq.(7):

$$\vec{j_i}' = \frac{\vec{j_i} l_0}{D_{i0}\rho_{i0}} = \mathrm{Sh} \tag{7}$$

where "Sh" is the Sherwood number and "$\vec{j_i}$" is the diffusion flux of specie "i" which arises due to its concentration gradient ($mol/m^{-2} \cdot s^{-1}$). Using Fick's law, it is possible to describe the mass diffusion flux as a function of the concentration gradient:

$$\vec{j_i} = -\rho_i D_i \nabla Y_i \tag{8}$$

where "Y_i" is the mass fraction of the specie "i".

The generalized reaction rate for each specie, for a unique non-reversible reaction is described by Eq.9:

$$R_i = M_{w,i}\left(\vartheta_j - \vartheta_i\right)\left(k_f \prod_{i=1}^{N} (C_i)^{(\eta_i)}\right) \tag{9}$$

where "$M_{w,i}$" is the molecular weight of the specie "i", "ϑ_j" and "ϑ_i" are the stoichiometric coefficients for product "j" and reactant "i"

respectively, "k_f" is the kinetic constant of the chemical reaction, "C_i" is the molar concentration of the component "i" and "η_i" is the reaction order for specie "i".

The numerical simulation has been carried out using a finite volume solver, ANSYS Fluent 19.2 (ANSYS, Inc., Canonsburg, PA, USA). A structured grid was defined and applied to discretize the computational domain. In order to capture the complex flow field in the vortex formation and the location of the interface between the two fluid streams, the geometry was meshed with a regular mesh using a multizone method where the mesh is refined in the radial direction to optimize the computational time.

The boundary conditions applied corresponded to normal velocity components at the inlets and atmospheric pressure at the outlet. No-slip boundary condition was assigned to the walls.

The chemical reaction was classified as a volumetric type reaction and the progress of the reaction was solved using a pressure-based approach in pseudo transient time using the Stiff Chemistry Solver. The solution method for the species is second order upwind and first order upwind for momentum and energy equations.

3. Materials and methods

3.1. Micro-reactor design

In this study, the performance of four different micro-reactor geometries has been studied. These three-dimensional geometries, which are shown in Fig. 1 have a circular cross section (radius = 0.4 mm) and a total length of 400 mm. All of them were designed in Autodesk Inventor® and fabricated with Tygon® tube with a 60° inlet angle between the two reagent inlets.

The straight reactor (Fig. 1.a) presents the simplest geometry of all, the rest of the geometries contain curves with different radii of curvature. For the serpentine 1 (Fig. 1.c) the radius of curvature is 13.6 mm and for the serpentine 2 (Fig. 1.d) this radius decreases to 2.7 mm. In the Archimedean spiral (Fig. 1.b), the radius of curvature is between 6.3 and 23.8 mm.

Details of the micro-reactor meshing can be found in the supplementary material.

3.2. Experimental section

Finally, for the experimental section different materials were required: ammonium solution was Panreac® (purity, 30%) and sodium hypochlorite was Labkem® (purity, 10%). The pH of the solutions was adjusted by adding sulfuric acid (Fisher Scientific®, purity ≥ 95%).

3.2.1. Kinetic study

For the kinetic study, batch experiments were performed; 10 ml of ammonium solution (1.1 mM) were contacted with 10 ml of hypochlorite solution (5.5 mM) under stirring at neutral pH. Samples (1 ml) were taken at known intervals of time and quenched by addition of ammonium test reagents (HI 93700, Hanna Instruments Company) in NaOH solution at pH = 13. The concentration of total ammonium was determined in a spectrophotometer (UV-1900, Shimadzu®) with a wavelength of 420 nm using commercial kits.

The oxidation of ammonium by hypochlorite has been reported to follow a second order kinetic equation, first order kinetics with respect to ammonium and first order with respect to hypochlorite anion, as expressed in Eq. (10).

$$-\frac{dC_{NH_4^+}}{dt} = k \cdot C_{NH_4^+} \cdot C_{ClO^-} \tag{10}$$

where "k" is the estimated value of the kinetic constant and "C" refers to reagents concentration.

3.2.2. Analysis of the micro-reactors performance

For the experimental analysis of the micro-reactors performance, two syringe pumps were used to feed the reagents; one syringe pumped the ammonium solution (1.1 mM) and the second syringe pumped the sodium hypochlorite solution (5.5 mM); the pH of both solutions was kept neutral by adding sulfuric acid. The syringes were connected to the micro-reactor Tygon® tube by a luer lock connector.

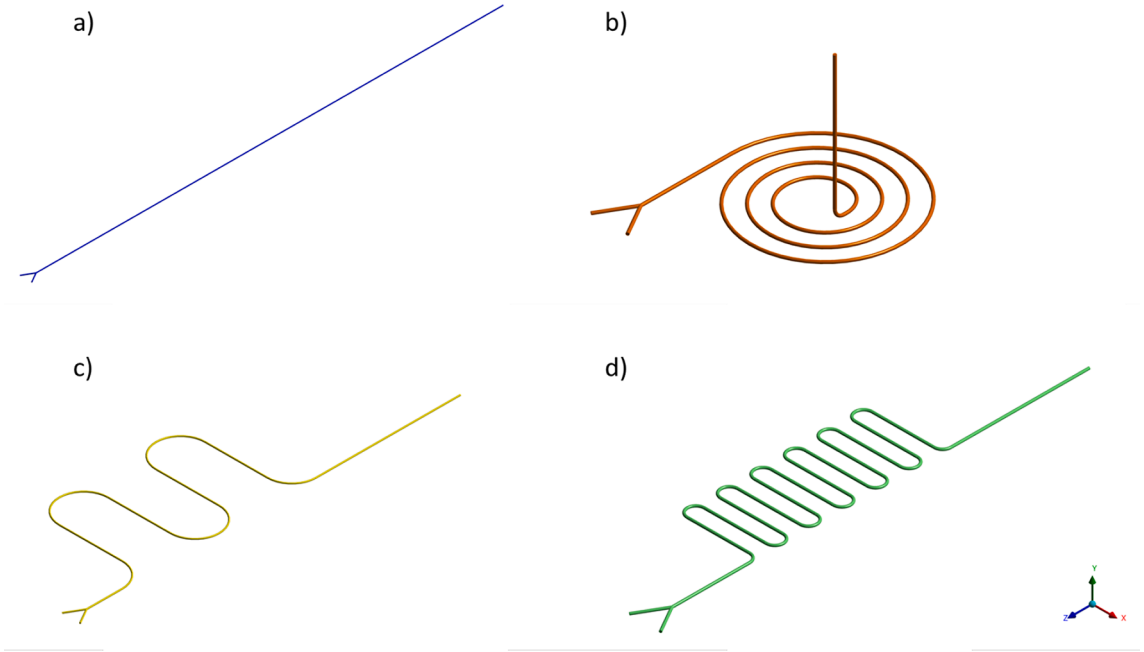

Fig. 1. 3D design of the different micro-reactor geometries: top left is a straight reactor, top right is an Archimedean spiral and the bottom two are serpentines, 1 and 2 respectively.

The flow rate was adjusted with both syringe pumps (Fig. 2.a) for each experiment maintaining the hypochlorite/ammonium molar ratio equal to 5:1 and flowing the same reagent flow rate through each inlet (between 0.2 and 6 ml·min-1). The micro-device was placed vertically with the outlet tube submerged in the NaOH solution in order to quench the reaction (by the same method that was employed to study the reaction kinetics) when leaving the micro-reactor. Samples (1 ml) were taken in a stirred vial (Fig. 2.c) at known residence times (sampling time vary between 10 s and 300 s, depending of the flow rate). Finally, the ammonium concentration at the outlet of the micro-reactor was measured in a UV-V spectrophotometer at a wavelength of 420 nm.

4. Results and discussion

In this study, ammonium oxidation by hypochlorite was employed as model reaction to characterise the performance of the different micro-reactor geometries. The reaction between the ammonium cation (NH_4^+) and the hypochlorous acid (HClO) is represented by the following stoichiometric equation [50]:

$$NH_4^+ + {}^3\!/_2\ HClO \rightarrow {}^1\!/_2 N_2 + {}^3\!/_2\ Cl^- + {}^3\!/_2\ H_2O + {}^5\!/_2 H^+ \qquad \text{R1}$$

First, the reaction kinetics between ammonium and hypochlorite at neutral pH with an initial molar ratio of 5 mol of hypochlorite for each mole of ammonium at room temperature (22 °C) was experimentally evaluated in batch experiments conducted under magnetic stirring.

With the experimental results, the value of the kinetic constant of the reaction was estimated using the Aspen Custom Modeler® parameter estimation tool obtaining a kinetic constant value of 156.6 ($sec^{-1}\cdot mole^{\cdot 1}\cdot L$) which is in accordance with the values previously reported in literature [51,52] and getting a very good fitting between experimental and simulated values with the estimated parameter (Fig. 3).

For CFD simulations, first, the influence of the mesh quality was analysed in the simulated ammonium concentration results. Fig. 4 shows the mesh quality study for the serpentine 2 micro-reactor where it is observed that in the range between 0 and $6{\cdot}10^5$ nodes, the number of nodes influences the simulated conversion of ammonium; however, from $6{\cdot}10^5$ nodes on there is no significant change in the ammonium conversion but the computational time increases drastically. When a mesh has a low number of nodes, the cell size is large giving rise to a low accuracy in the location of the interface that translates in the over-estimation of the mixing within the micro-reactor and consequently in the calculated ammonium conversion increase.

For the operational conditions used in this work, it was estimated the diffusion coefficient of the ammonium ion as $D = 1.79{\cdot}10^{-9}\ m^2{\cdot}s^{-1}$ [53].

Results of the performance for different geometries are expressed as ammonium conversion and depicted in Fig. 5; in this figure the experimental results are given together with the simulated curve corresponding to ideal behaviour, that is when there is no influence of the mixture since the inlet streams enter the reactor fully mixed.

As shown in Fig. 5, when the residence time is very low (τ less than 5 s), the performance of the curved micro-reactors is similar to that of the pre-mixed reactor, because the convection mixing occurs in curved geometries and the overall performance is controlled by the chemical reaction rate. On the other hand, for the straight reactor with no curves, no convection mixing occurs and the performance of the micro-device is limited by molecular diffusion. Then, in order to achieve the mixing degree the average residence time in the micro-device should be equal to the diffusion time [54]:

$$t_{res} = t_{diff} \qquad (11)$$

$$\frac{L}{u} = \frac{L_{mix}^2}{2D_i} \qquad (12)$$

Considering typical values for the diffusivity of solutes in liquid phase, mixing length and velocities inside the microfluidic devices, the required mixing channel usually results unacceptably long for the straight reactor to achieve high conversions.

As residence time increases, the inertial forces inside the micro-reactor become less important, therefore molecular diffusion is the mixing controlling mechanism in all geometries.

Furthermore, as the curvature radius decreases it favours ammonium oxidation, for instance, at a residence time of 10 s, the conversion is 48% in the case of the straight reactor, 75% of serpentine 1, 80% of serpentine 2, and 86% of the Archimedean spiral. For instance, to achieve an ammonium conversion of 90% the spiral shape micro-reactor needs 14 s of residence time, while residence times of 18, 12 and 8 s are required for the straight reactor, serpentine 1 and 2 respectively, to achieve the same conversion compared to the spiral geometry.

In order to gain insight on how mixing affects the micro-reactor's

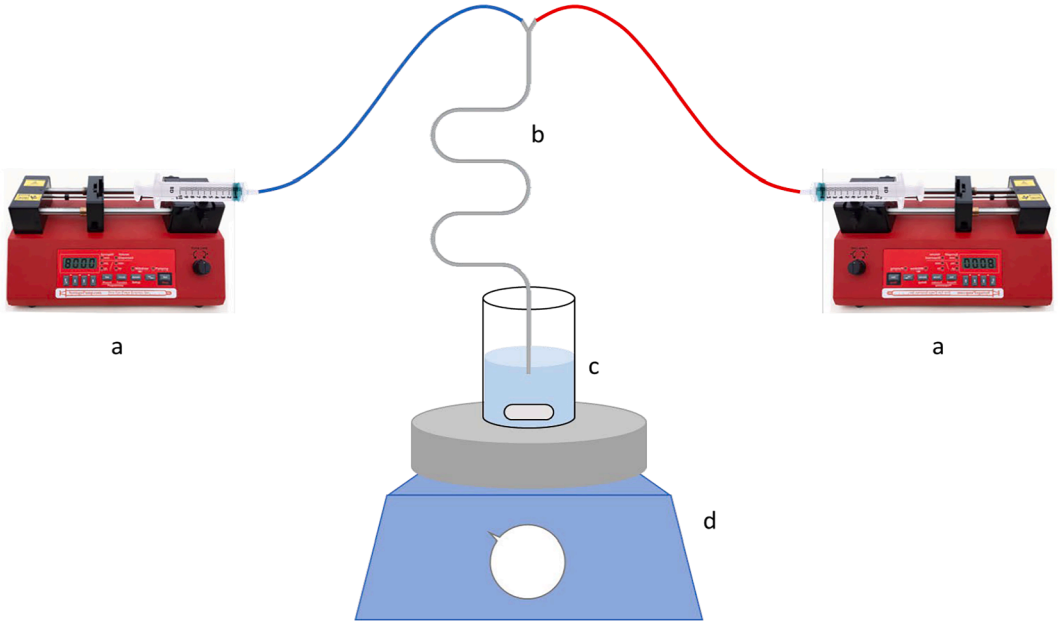

Fig. 2. Experimental diagram for the analysis of the micro-reactor performance, composed of two syringe pumps (a), the micro-reactor (b), stirred glass vial (c) and magnetic stirrer (d).

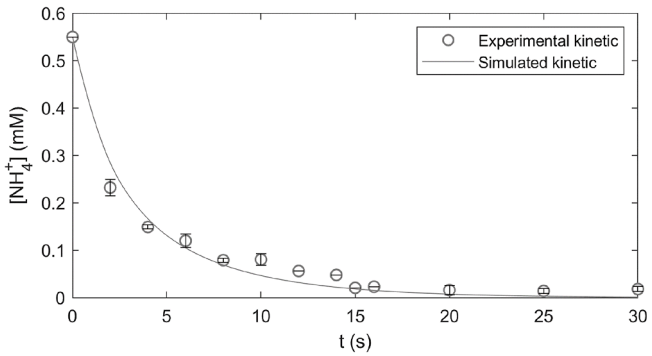

Fig. 3. Comparison between the simulated and experimental kinetic data represented by the line and dots, respectively at 22 °C and pH = 7 with 5:1 M ratio [HClO]/[NH_4^+]. Total volume of 20 ml.

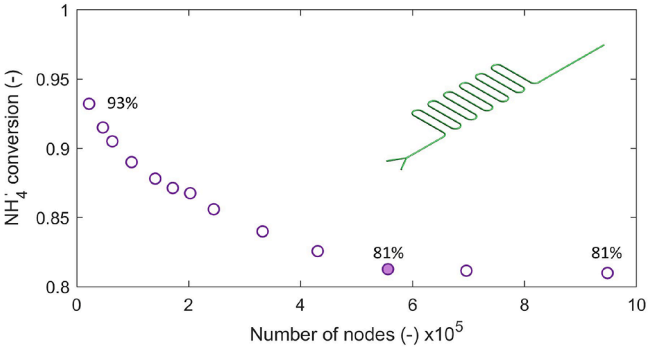

Fig. 4. Mesh quality study for the serpentine 2 micro-reactor.

performance the mixing pattern along the length of the device has been studied. The mixing degree was estimated by calculating the variance of the concentration on a particular transversal plane normal to the fluid flow [55–57]. The variance of the mass fraction was determined as:

$$\sigma = \sqrt{\frac{1}{N\bar{u}}\sum_{i=1}^{N}(\phi_i - \overline{\phi_b})^2 u_i} \tag{13}$$

where "N" is the number of sampling points within the cross-sectional plane, "ϕ_i" is the mass fraction of fluid at point "i", "$\overline{\phi_b}$" denotes the cup mixing average mass fraction, "u_i" and "$\bar{u}$" represent the axial velocity at point "i" and mean velocity respectively. The mixing index was defined as:

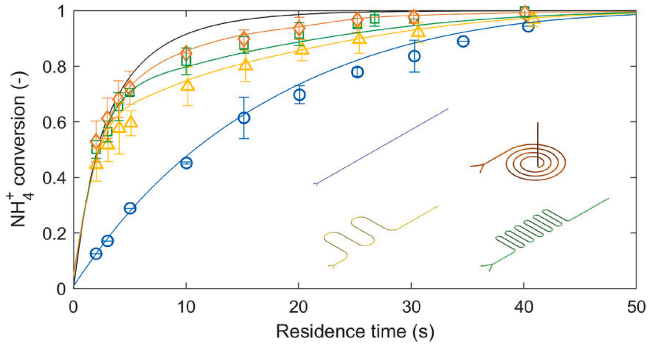

Fig. 5. Ammonium conversion as function of the residence time in the micro-reactors with different geometries. – pre-mixed reactor, ◇ Spiral, □ Serpentine 2, △ Serpentine 1, ○ Straight reactor. Dots and lines represent experimental and simulated data respectively.

$$MI = 1 - \frac{\sigma}{\sigma_{max}} \tag{14}$$

where "σ_{max}" is the maximum variance over the range.

Fig. 6 shows the mixing degree achieved with different micro-device geometries for a specific residence time ($\tau = 10$ s), observing that the mixture in the spiral shape was improved, in terms of the mixing index, by 58%, 28% and 18% compared to straight reactor, serpentine 1 and 2 respectively.

The different mixing degrees are caused by the curved micro-channels, where chaotic advection is induced by the action of the centripetal forces that cause the fluid molecules to change their main direction of motion. This gives rise to a secondary motion, perpendicular to the main flow direction, in which the fluid in the centre of the pipe is pushed towards the outer side of the bend and the fluid near the pipe wall is forced to return to the inner part of the channel. This secondary motion is developed as a pair of counter-rotating cells, which are called Dean vortices. This phenomenon is characterized by the Dean number (De).

$$De = \frac{\sqrt{\frac{1}{2}(centripetal\ forces)(intertial\ forces)}}{viscousforces} = Re\sqrt{\frac{d_h}{2r_c}} \tag{15}$$

Where "d_h" is the hydraulic diameter of the micro-channel (m) and "r_c" is the curvature radius of the channel (m).

The worst performance was obtained with the straight reactor, where the mixture is only generated by molecular diffusion. The performance of the serpentine's 1 is significantly improved compared to the previous one. This is because a curved geometry induces the generation of passive mixture due to the appearance of Dean's vortices (Fig. 7).

The performance of serpentine 2 appears slightly improved compared to the serpentine 1, because despite having a shorter curved length (102 mm, 25.5% of the total length for serpentine 1, compared to serpentine 2 that has 171 mm of curvature, 43% of the total length), the inertial forces produced by the smaller curvature radius generate more efficient Dean vortices improving the performance of the passive mixing (De = 5.5 and 12.3 for serpentine 1 and 2 respectively with $\tau = 10$ s). The best performance was achieved with the spiral shape since Dean vortices are efficiently generated (De oscillate between: 4.1 and 8.1 for $\tau = 10$ s) and this geometry has 338 mm of curved length, which means that Dean vortices are being generated at 84.5% of the length and consequently throughout that length mixing takes place by convection.

Finally, using computational fluid dynamics (CFD) techniques with Ansys Fluent®, the performance of the system has been predicted obtaining good agreement between simulated data and experimental results, concluding that the mathematical model predicts the system with an error of less than 10% in 100% of the cases (Fig. 8). The points that are out of the selected range of agreement correspond to the highest flow rate, where the experimental error is higher.

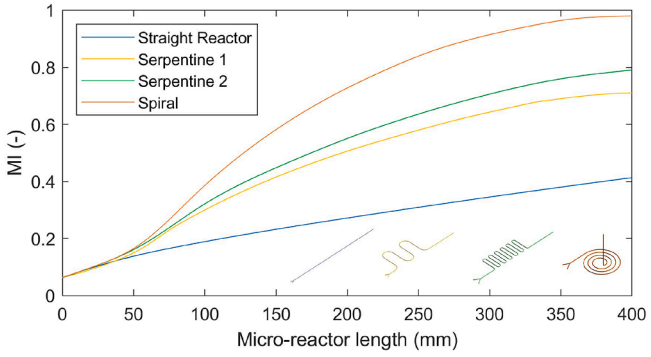

Fig. 6. Simulated Mixing Index (MI) along the length in micro-reactors with different geometries for 10 s of residence time. ● Spiral, ● Serpentine 2, ● Serpentine 1, ● Straight reactor.

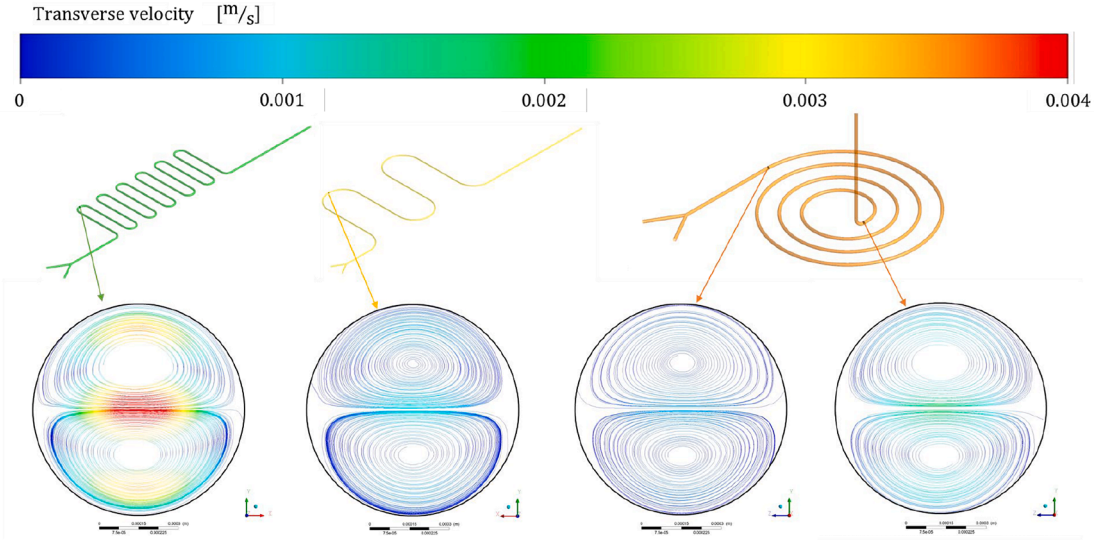

Fig. 7. Velocity lines in the curved part that cause the generation of vortices within the micro-reactors for different configurations: Serpentine 1, Serpentine 2, Spiral with a residence time of 10 s.

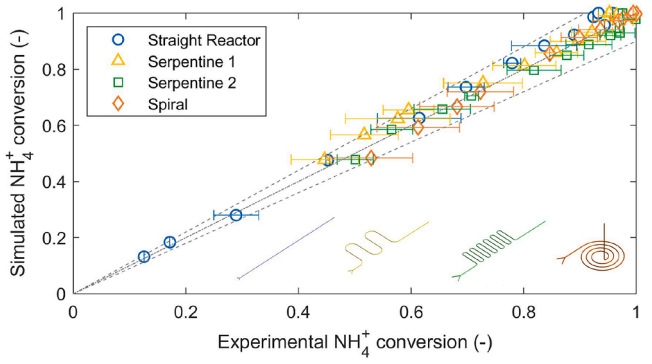

Fig. 8. Parity plot with a ± 10% error (grey dashed lines) between the experimental values and the mathematical model simulations of each micro-reactor Spiral, Serpentine 1, Serpentine 2, Straight reactor.

5. Conclusions

A detailed holistic study of chemical reaction and mixing performance in different micro-device geometries has been performed using experimental and numerical simulation techniques. The main objective of this work is to understand the phenomena that govern the fluid dynamics in curved micro-channels and the coupling with chemical reaction kinetics to develop a tool that allows the design of micro-reactors for different liquid-phase applications.

The best performance was obtained with the spiral shape micro-reactor, improving the ammonium conversion by 44%, 12% and 7% with respect to the straight reactor, serpentines 1 and 2 respectively, for a residence time of 10 s. This improvement is explained because the spiral geometry has the best trade-off between the curvature radius and curved length compared with other geometries.

The curves in micro-reactors geometry bring about the appearance of the Dean vortices, causing a secondary movement perpendicular to the direction of the main flow, that improves the mixing degree within the micro-device by generating convective mixing. Therefore, the mixing degree increases with increasing the curved length where Dean vortices are generated, and with decreasing the curvature radius that favour the formation of more efficient Dean vortices.

In addition, a mathematical model has been developed in Ansys Fluent® employing computational fluid dynamics (CFD) techniques; the model is capable to accurately predict the performance of different micro-reactor geometries. This model has been experimentally validated with different micro-devices configurations employing a fast second order reaction with an error between experimental and simulated data of less than 10%.

Thus, we report a valuable tool to assist in the design of micro-reactors that accounts for the integrated analysis of reactants mixing and reaction rate; this tool allows predicting the performance of different geometries and facilitates the decision-making of the process conditions for liquid-phase reactions.

Dimensionless numbers:

$$\mathrm{S} = \frac{\text{temporal variation}}{\text{convection}} = \frac{l_0}{\vec{v_0} t_0} \rightarrow \text{Strouhal number}$$

$$\mathrm{Eu} = \frac{\text{pressure forces}}{\text{inertial forces}} = \frac{\Delta p_0}{\rho_0 \vec{v_0}^2} \rightarrow \text{Euler number}$$

$$\mathrm{Re} = \frac{\text{convection}}{\text{diffusion}} \approx \frac{\text{inertial forces}}{\text{viscous forces}} = \frac{\rho_0 \vec{v_0} l_0}{\mu_0} \rightarrow \text{Reynolds number}$$

$$\mathrm{Sh} = \frac{\text{convective mass transfer rate}}{\text{diffusion mass transport rate}} = \frac{\vec{j_i} l_0}{D_{i0} \rho_{i0}} \rightarrow \text{Sherwood number}$$

$$\mathrm{Pe} = \frac{\text{mass transfer of component } i \text{ by convection}}{\text{mass transfer of component } i \text{ by diffusion}} = \frac{\vec{v_0} l_0}{D_{A0}} \rightarrow \text{Peclet number}$$

$$\mathrm{Da} = \frac{\text{production of component } i}{\text{convection}} = \frac{R_{i0} l_0}{\rho_{i0} \vec{v_0}} = \text{Damköhler number}$$

$$\mathrm{Fr} = \frac{\text{inertial forces}}{\text{body forces}} = \frac{\vec{v_0}}{\sqrt{g l_0}} = \text{Froude number}$$

Declaration of Competing Interest

The authors declare that they have no known competing financial interests or personal relationships that could have appeared to influence the work reported in this paper.

Acknowledgements

Financial assistance from the project RTI2018-093310-B-I00 (MCI/AEI/FEDER,UE) is gratefully acknowledged.

Appendix A. Supplementary data

Supplementary data to this article can be found online at https://doi.org/10.1016/j.cej.2022.135192.

References

[1] G.M. Whitesides, The origins and the future of microfluidics, Nature. 442 (7101) (2006) 368–373, https://doi.org/10.1038/nature05058.

[2] T. Sprogies, J.M. Köhler, G.A. Groß, Evaluation of static micromixers for flow-through extraction by emulsification, Chem. Eng. J. 135 (2008) 200–203, https://doi.org/10.1016/j.cej.2007.07.032.

[3] A. Basauri, J. Gomez-Pastora, M. Fallanza, E. Bringas, I. Ortiz, Predictive model for the design of reactive micro-separations, Sep. Purif. Technol. 209 (2019) 900–907, https://doi.org/10.1016/j.seppur.2018.09.028.

[4] J. Gómez-Pastora, C. González-Fernández, M. Fallanza, E. Bringas, I. Ortiz, Flow patterns and mass transfer performance of miscible liquid-liquid flows in various microchannels: Numerical and experimental studies, Chem. Eng. J. 344 (2018) 487–497, https://doi.org/10.1016/j.cej.2018.03.110.

[5] A. Farahani, A. Rahbar-Kelishami, H. Shayesteh, Microfluidic solvent extraction of Cd(II) in parallel flow pattern: Optimization, ion exchange, and mass transfer study, Sep. Purif. Technol. 258 (2021) 118031, https://doi.org/10.1016/j.seppur.2020.118031.

[6] C. González Fernández, J. Gómez Pastora, A. Basauri, M. Fallanza, E. Bringas, J. J. Chalmers, I. Ortiz, Continuous-flow separation of magnetic particles from biofluids: How does the microdevice geometry determine the separation performance? Sensors (Switzerland). 20 (11) (2020) 3030, https://doi.org/10.3390/s20113030.

[7] W. Low, N. Kadri, Computational analysis of enhanced circulating tumour cell (CTC) separation in a microfluidic system with an integrated dielectrophoretic-magnetophorectic (DEP-MAP) technique, Chemosensors. 4 (3) (2016) 14, https://doi.org/10.3390/chemosensors4030014.

[8] D. Ma, C. Zhu, T. Fu, X. Yuan, Y. Ma, An effective hybrid solvent of MEA/DEEA for CO2 absorption and its mass transfer performance in microreactor, Sep. Purif. Technol. 242 (2020) 116795, https://doi.org/10.1016/j.seppur.2020.116795.

[9] Y. Yin, X. Zhang, C. Zhu, T. Fu, Y. Ma, Hydrodynamics and gas-liquid mass transfer in a cross-flow T-junction microchannel: Comparison of two operation modes, Sep. Purif. Technol. 255 (2021) 117697, https://doi.org/10.1016/j.seppur.2020.117697.

[10] C.-Y. Hou, L.-M. Fu, W.-J. Ju, P.-Y. Wu, Microfluidic colorimetric system for nitrite detection in foods, Chem. Eng. J. 398 (2020) 125573, https://doi.org/10.1016/j.cej.2020.125573.

[11] T. Zhang, Y. He, J. Wei, L. Que, Nanostructured optical microchips for cancer biomarker detection, Biosens. Bioelectron. 38 (1) (2012) 382–388, https://doi.org/10.1016/j.bios.2012.06.029.

[12] K.T.L. Trinh, R.A. Stabler, N.Y. Lee, Fabrication of a foldable all-in-one point-of-care molecular diagnostic microdevice for the facile identification of multiple pathogens, Sensors Actuators, B Chem. 314 (2020) 128057, https://doi.org/10.1016/j.snb.2020.128057.

[13] P. Derboven, P.H.M. Van Steenberge, J. Vandenbergh, M.-F. Reyniers, T. Junkers, D.R. D'hooge, G.B. Marin, Improved Livingness and Control over Branching in RAFT Polymerization of Acrylates: Could Microflow Synthesis Make the Difference? Macromol. Rapid Commun. 36 (24) (2015) 2149–2155, https://doi.org/10.1002/marc.201500357.

[14] G. Chen, S. Li, F. Jiao, Q. Yuan, Catalytic dehydration of bioethanol to ethylene over TiO2/γ-Al2O3 catalysts in microchannel reactors, Catal. Today. 125 (1-2) (2007) 111–119, https://doi.org/10.1016/j.cattod.2007.01.071.

[15] N. Wang, X. Zhang, Y.u. Wang, W. Yu, H.L.W. Chan, Microfluidic reactors for photocatalytic water purification, Lab Chip. 14 (6) (2014) 1074–1082.

[16] H.J. Venvik, J. Yang, Catalysis in microstructured reactors: Short review on small-scale syngas production and further conversion into methanol, DME and Fischer-Tropsch products, Catal. Today. 285 (2017) 135–146, https://doi.org/10.1016/j.cattod.2017.02.014.

[17] S. Kim, H. Wang, L. Yan, X. Zhang, Y.i. Cheng, Continuous preparation of itraconazole nanoparticles using droplet-based microreactor, Chem. Eng. J. 393 (2020) 124721, https://doi.org/10.1016/j.cej.2020.124721.

[18] T. Hong, A. Lu, W. Liu, C. Chen, Microdroplet synthesis of silver nanoparticles with controlled sizes, Micromachines. 10 (4) (2019) 274, https://doi.org/10.3390/mi10040274.

[19] C.-X. Zhao, L. He, S.Z. Qiao, A.P.J. Middelberg, Nanoparticle synthesis in microreactors, Chem. Eng. Sci. 66 (7) (2011) 1463–1479, https://doi.org/10.1016/j.ces.2010.08.039.

[20] A. Bogdan, S. Poe, D. Kubis, S. Broadwater, D.T. McQuade, The continuous-flow synthesis of ibuprofen, Angew. Chemie - Int. Ed. 48 (45) (2009) 8547–8550, https://doi.org/10.1002/anie.200903055.

[21] B. Gutmann, D. Cantillo, C.O. Kappe, Continuous-flow technology - A tool for the safe manufacturing of active pharmaceutical ingredients, Angew. Chemie - Int. Ed. 54 (23) (2015) 6688–6728, https://doi.org/10.1002/anie.201409318.

[22] H.-J. Lee, H. Kim, D.-P. Kim, From p-Xylene to Ibuprofen in Flow: Three-Step Synthesis by a Unified Sequence of Chemoselective C−H Metalations, Chem. - A Eur. J. 25 (50) (2019) 11641–11645, https://doi.org/10.1002/chem.201903267.

[23] J.S. Zhang, Y.C. Lu, Q.R. Jin, K. Wang, G.S. Luo, Determination of kinetic parameters of dehydrochlorination of dichloropropanol in a microreactor, Chem. Eng. J. 203 (2012) 142–147, https://doi.org/10.1016/j.cej.2012.07.061.

[24] P. Wang, K. Wang, J. Zhang, G. Luo, Kinetic study of reactions of aniline and benzoyl chloride in a microstructured chemical system, AIChE J. 61 (11) (2015) 3804–3811, https://doi.org/10.1002/aic.14891.

[25] J.P. McMullen, K.F. Jensen, Rapid determination of reaction kinetics with an automated microfluidic system, Org. Process Res. Dev. 15 (2) (2011) 398–407, https://doi.org/10.1021/op100300p.

[26] Y. Zhang, J. Li, Y. Jin, M. Chen, Y. Wang, Determination of kinetic parameters of homogenous continuous flow esterification of monobutyl chlorophosphate in a microreactor, Can. J. Chem. Eng. 98 (5) (2020) 1139–1147.

[27] P.L. Suryawanshi, S.P. Gumfekar, B.A. Bhanvase, S.H. Sonawane, M.S. Pimplapure, A review on microreactors: Reactor fabrication, design, and cutting-edge applications, Chem. Eng. Sci. 189 (2018) 431–448, https://doi.org/10.1016/j.ces.2018.03.026.

[28] M. Baumann, I.R. Baxendale, The synthesis of active pharmaceutical ingredients (APIs) using continuous flow chemistry, Beilstein J. Org. Chem. 11 (2015) 1194–1219, https://doi.org/10.3762/bjoc.11.134.

[29] N. Miložič, M. Lubej, M. Lakner, P. Žnidaršič-Plazl, I. Plazl, Theoretical and experimental study of enzyme kinetics in a microreactor system with surface-immobilized biocatalyst, Chem. Eng. J. 313 (2017) 374–381, https://doi.org/10.1016/j.cej.2016.12.030.

[30] K. Ward, Z.H. Fan, Mixing in microfluidic devices and enhancement methods, J. Micromechanics Microengineering. 25 (9) (2015) 094001, https://doi.org/10.1088/0960-1317/25/9/094001.

[31] K.K. Gill, R. Gibson, K.H.C. Yiu, P. Hester, N.M. Reis, Microcapillary film reactor outperforms single-bore mesocapillary reactors in continuous flow chemical reactions, Chem. Eng. J. 408 (2021) 127860, https://doi.org/10.1016/j.cej.2020.127860.

[32] M.J. Nieves-Remacha, A.A. Kulkarni, K.F. Jensen, Hydrodynamics of liquid-liquid dispersion in an advanced-flow reactor, Ind. Eng. Chem. Res. 51 (50) (2012) 16251–16262, https://doi.org/10.1021/ie301821k.

[33] M.D. Tarn, N. Pamme, On-chip magnetic particle-based immunoassays using multilaminar flow for clinical diagnostics (2017), https://doi.org/10.1007/978-1-4939-6734-6_6.

[34] J. Gómez-Pastora, V. Amiri Roodan, I.H. Karampelas, A.Q. Alorabi, M.D. Tarn, A. Iles, E. Bringas, V.N. Paunov, N. Pamme, E.P. Furlani, E.P. Furlani, I. Ortiz, Two-Step Numerical Approach to Predict Ferrofluid Droplet Generation and Manipulation inside Multilaminar Flow Chambers, J. Phys. Chem. C. 123 (2019) 10065–10080, https://doi.org/10.1021/acs.jpcc.9b01393.

[35] K.K. Gill, Z. Liu, N.M. Reis, Fast prototyping using 3D printed templates and flexible fluoropolymer microcapillary films offers enhanced micromixing in immobilised (bio)catalytic reactions, Chem. Eng. J. 429 (2022) 132266, https://doi.org/10.1016/j.cej.2021.132266.

[36] S. Wong, M. Ward, C. Wharton, Micro T-mixer as a rapid mixing micromixer, Sensors Actuators, B Chem. 100 (3) (2004) 359–379, https://doi.org/10.1016/j.snb.2004.02.008.

[37] S. Camarri, A. Mariotti, C. Galletti, E. Brunazzi, R. Mauri, M.V. Salvetti, An Overview of Flow Features and Mixing in Micro T and Arrow Mixers, Ind. Eng. Chem. Res. 59 (9) (2020) 3669–3686, https://doi.org/10.1021/acs.iecr.9b04922.

[38] M. Nimafar, V. Viktorov, M. Martinelli, Experimental comparative mixing performance of passive micromixers with H-shaped sub-channels, Chem. Eng. Sci. 76 (2012) 37–44, https://doi.org/10.1016/j.ces.2012.03.036.

[39] V. Viktorov, M.R. Mahmud, C. Visconte, Numerical study of fluid mixing at different inlet flow-rate ratios in Tear-drop and Chain micromixers compared to a new H-C passive micromixer, Eng. Appl. Comput. Fluid Mech. 10 (1) (2016) 182–192, https://doi.org/10.1080/19942060.2016.1140075.

[40] S.-S. Hsieh, J.-W. Lin, J.-H. Chen, Mixing efficiency of Y-type micromixers with different angles, Int. J. Heat Fluid Flow. 44 (2013) 130–139, https://doi.org/10.1016/j.ijheatfluidflow.2013.05.011.

[41] A.S. Yang, F.C. Chuang, C.K. Chen, M.H. Lee, S.W. Chen, T.L. Su, Y.C. Yang, A high-performance micromixer using three-dimensional Tesla structures for bio-applications, Chem. Eng. J. 263 (2015) 444–451, https://doi.org/10.1016/j.cej.2014.11.034.

[42] S. Hossain, M.A. Ansari, A. Husain, K.-Y. Kim, Analysis and optimization of a micromixer with a modified Tesla structure, Chem. Eng. J. 158 (2) (2010) 305–314, https://doi.org/10.1016/j.cej.2010.02.002.

[43] H. Alijani, A. Özbey, M. Karimzadehkhouei, A. Koşar, Inertial micromixing in curved serpentine micromixers with different curve angles, Fluids. 4 (4) (2019) 204, https://doi.org/10.3390/fluids4040204.

[44] V.S. Duryodhan, R. Chatterjee, S. Govind Singh, A. Agrawal, Mixing in planar spiral microchannel, Exp. Therm. Fluid Sci. 89 (2017) 119–127, https://doi.org/10.1016/j.expthermflusci.2017.07.024.

[45] D. Ghosh, A.B. Vir, G. Garnier, A.F. Patti, J. Tanner, Continuous flow production of xylooligosaccharides by enzymatic hydrolysis, Chem. Eng. Sci. 244 (2021) 116789, https://doi.org/10.1016/j.ces.2021.116789.

[46] X. Chen, S. Liu, Y. Chen, S. Wang, A review on species mixing in droplets using passive and active micromixers, Int. J. Environ. Anal. Chem. 101 (3) (2021) 422–432, https://doi.org/10.1080/03067319.2019.1666832.

[47] M. Bayareh, M.N. Ashani, A. Usefian, Active and passive micromixers: A comprehensive review, Chem. Eng. Process. - Process Intensif. 147 (2020) 107771, https://doi.org/10.1016/j.cep.2019.107771.

[48] C.Y. Lee, W.T. Wang, C.C. Liu, L.M. Fu, Passive mixers in microfluidic systems: A review, Chem. Eng. J. 288 (2016) 146–160, https://doi.org/10.1016/j.cej.2015.10.122.

[49] G. Hauke, An Introduction to Fluid Mechanics and Transport Phenomena, Springer Science+Business Media, B. V., Zaragoza, 2008.

[50] Y. Gendel, O. Lahav, Revealing the mechanism of indirect ammonia electrooxidation, Electrochim. Acta. 63 (2012) 209–219, https://doi.org/10.1016/j.electacta.2011.12.092.
[51] A. Romano, I. Ortiz, A.M. Urtiaga, Comprehensive kinetics of electrochemically assisted ammonia removal in marine aquaculture recirculating systems, J. Electroanal. Chem. 897 (2021) 115619, https://doi.org/10.1016/j.jelechem.2021.115619.
[52] A. Romano, A.M. Urtiaga, I. Ortiz, Optimized energy consumption in electrochemical-based regeneration of RAS water, Sep. Purif. Technol. 240 (2020) 116638, https://doi.org/10.1016/j.seppur.2020.116638.
[53] J. Winkelmann, Diffusion in Gases, Liquids and Electrolytes, Springer, Berlin Heidelberg, Berlin, Heidelberg (2018), https://doi.org/10.1007/978-3-662-54089-3.
[54] H. Bruus, Theorethical Microfluids, Oxford University Press, New York, 2008.
[55] R. Byron Bird, W.E. Stewart, E.N. Lightfoot, Transport Phenomena, 2nd ed.,, John Wiley & Sons Inc, New York, 2002.
[56] W. Raza, S. Hossain, K.-Y. Kim, A review of passive micromixers with a comparative analysis, Micromachines. 11 (5) (2020) 455.
[57] G. Orsi, M. Roudgar, E. Brunazzi, C. Galletti, R. Mauri, Water-ethanol mixing in T-shaped microdevices, Chem. Eng. Sci. 95 (2013) 174–183, https://doi.org/10.1016/j.ces.2013.03.015.